Supplementary Information

Structural Phase Transition and Distortion-Mode Evolution in the One-Dimensional [$CuBr_4$] Chain Structure of $RbCu_2Br_3$

Authors:

Yousra Chakroun[a,b], Wajdi Cherif[c], Carlos A. López[a,d], Lilia Ktari[b], Brenda Martinelli[e], Javier Gainza[f], F. Serrano-Sánchez[a], Mateus M. Ferrer[e], Carlos Pecharromán[a], José Luis Martínez[a], María Teresa Fernández-Díaz[f], João Elias F. S. Rodrigues[a,g*], and José Antonio Alonso[a,*]

Affiliations:

[(a)] *Instituto de Ciencia de Materiales de Madrid, CSIC, Cantoblanco 28049 Madrid, Spain.*

[(b)] *Laboratory of Inorganic Chemistry, Faculty of Sciences of Sfax, University of Sfax. 3000 Sfax, Tunisia*

[(c)] *National Engineering School of Sfax (ENIS), Laboratory of Electromechanical Systems (LASEM), B.P.W. 3038, Sfax, Tunisia*

[(d)] *Instituto de Investigaciones en Tecnología Química (UNSL-CONICET) and Facultad de Química, Bioquímica y Farmacia, Almirante Brown 1455 (5700) San Luis, Argentina.*

[(e)] *CCAF, PPGCEM/CDTec, Federal University of Pelotas, 96010-610 Pelotas, Rio Grande do Sul, Brazil.*

[(f)] *Institut Laue Langevin. 38042 Grenoble Cedex, France*

[(g)] *ESRF – European Synchrotron Radiation Facility, 38000 Grenoble, France.*

Correspondence:

*ja.alonso@icmm.csic.es (JAA); rodrigues.joaoelias@gmail.com (JEFSR).

I. Chemical and morphological analyses

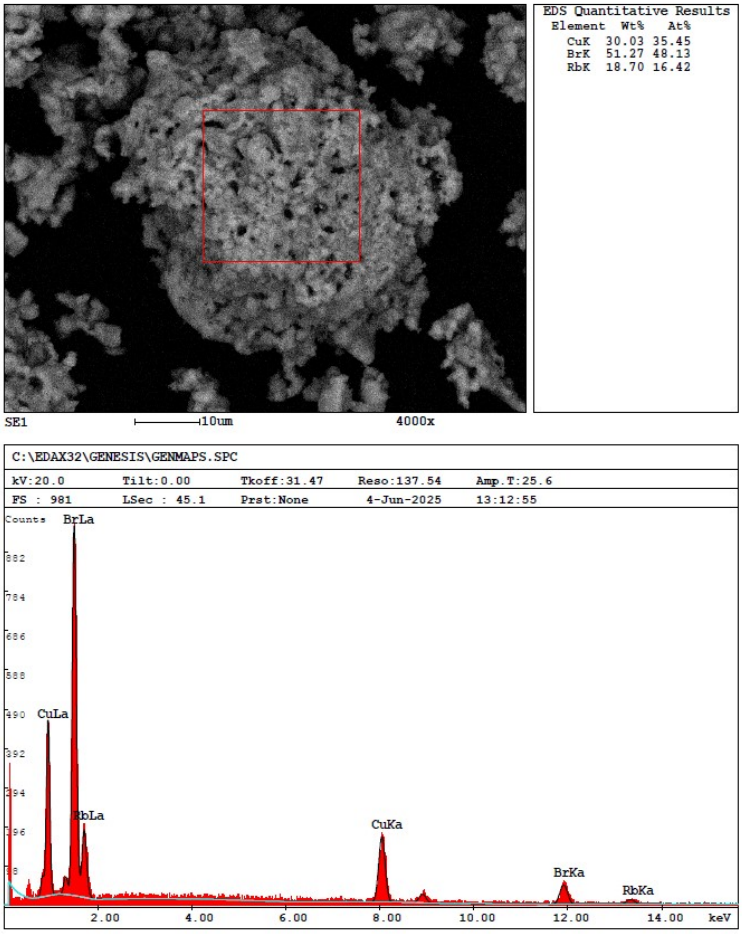

Fig. S1: Upper panel: SEM image where the EDXS spectrum was collected, and relative contents of Rb, Cu, and Br, very close to the expected composition $RbCu_2Br_3$. Lower panel: typical EDXS spectrum.

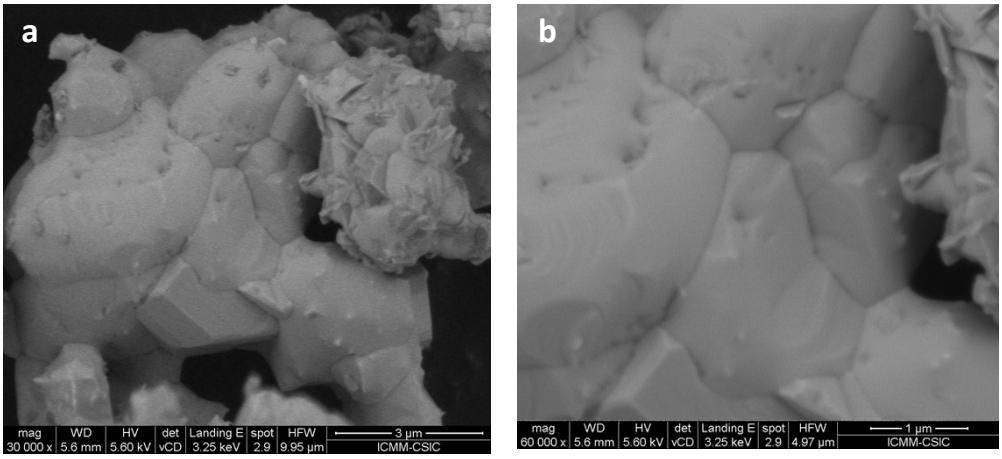

Fig. S2: FE-SEM images with (a) 30,000× and (b) 60,000x magnification.

II. Complementary structural data

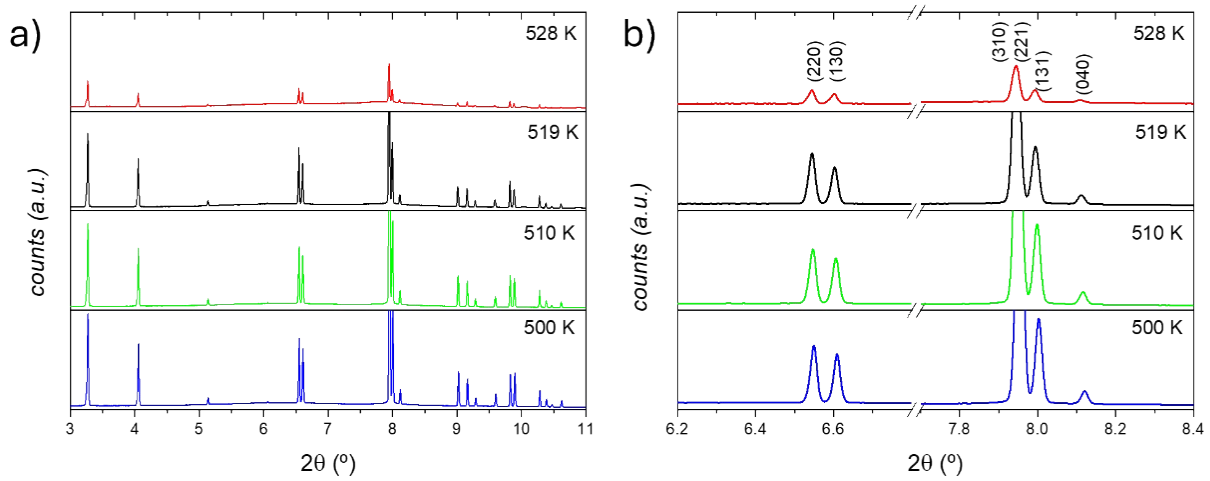

Fig. S3: Selected synchrotron XRD patterns above room temperature (MSPD, ALBA Synchrotron).

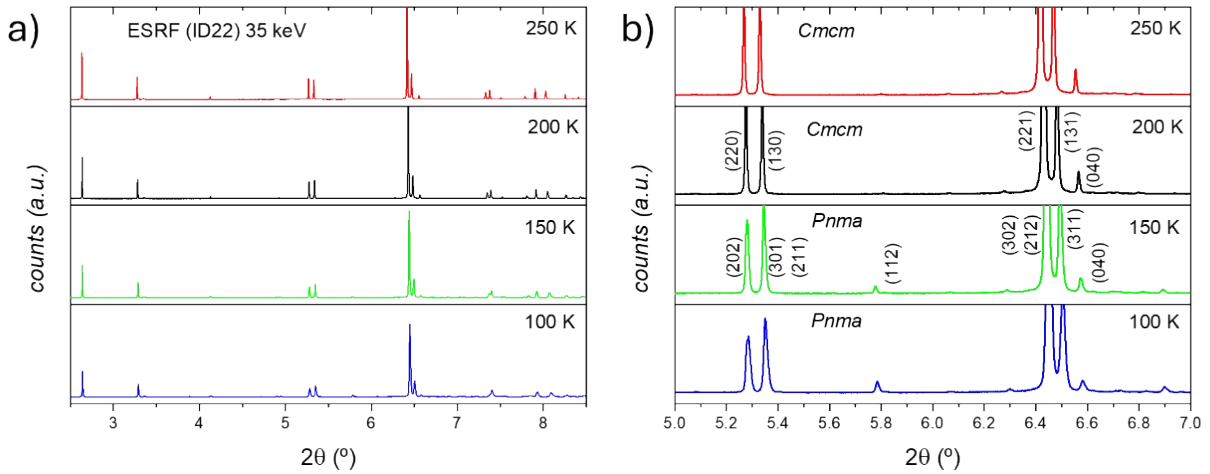

Fig. S4: Selected synchrotron XRD pattern below room temperature (ID22, ESRF).

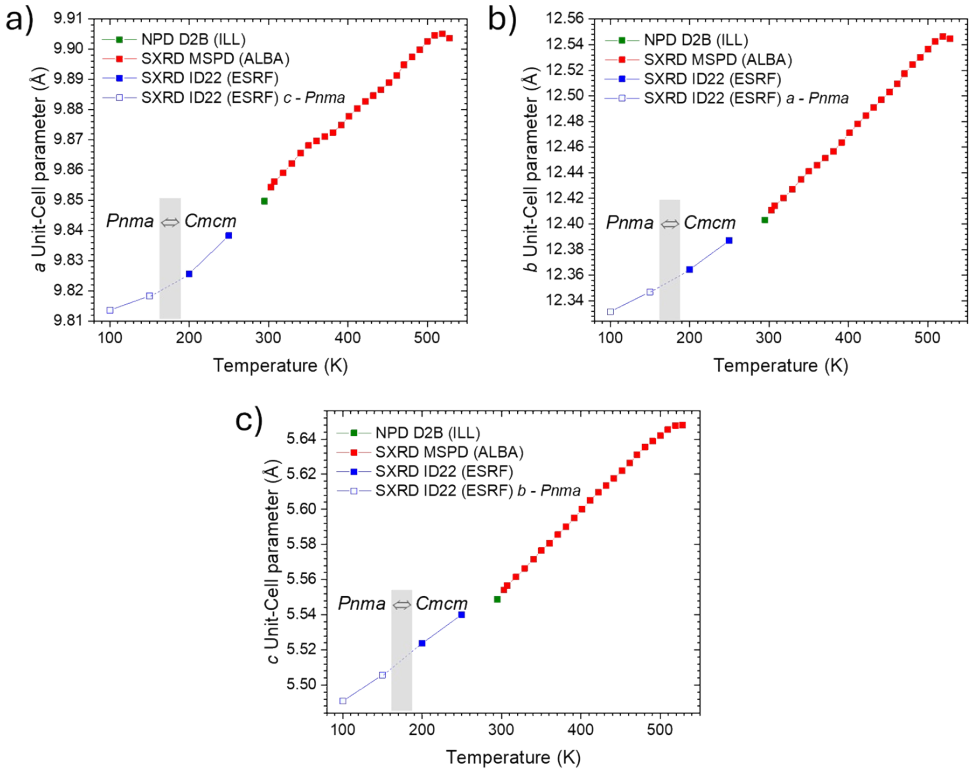

Fig. S5: Thermal evolution of unit-cell parameters: (a) *a*, (b) *b*, and (c) *c*.

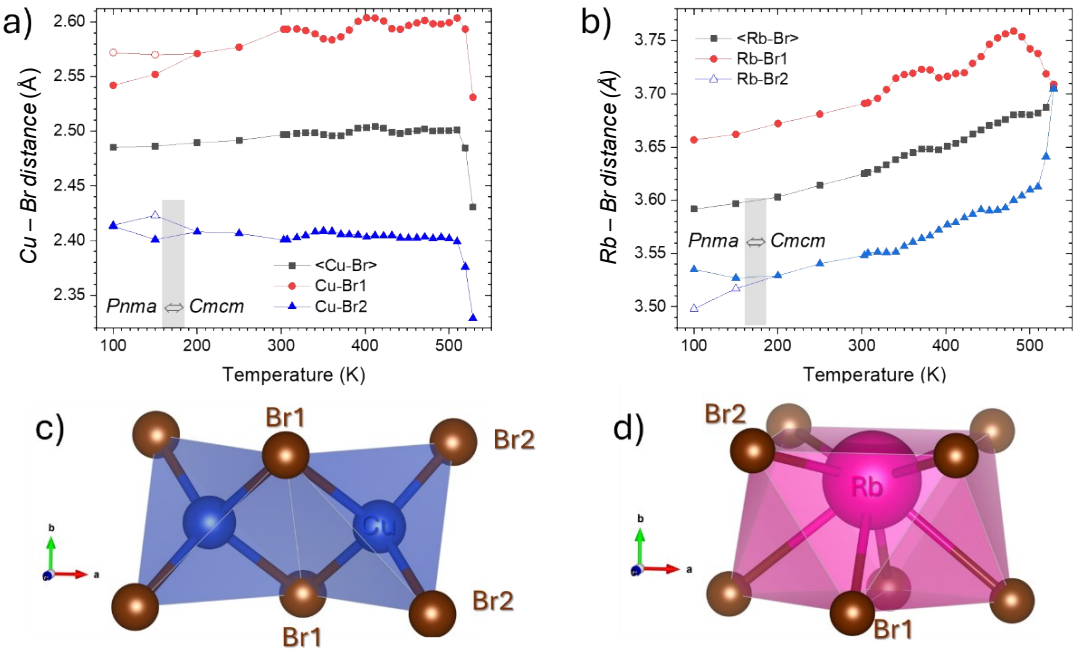

Fig. S6: Thermal evolution of interatomic distances (a) Cu–Br and (b) Rb–Br. Local representation of the (c) [$CuBr_4$] dimer and (d) [$RbBr_8$] units.

Table S1: Crystallographic data for $RbCu_2Br_3$ phase in the orthorhombic $Cmcm$ space-group from SXRD at 303 K. Unit-cell parameters: a = 9.85438(5) Å, b = 12.41065(6) Å, c = 5.55399(3) Å, and V = 679.249(6) Å^3.

Atom	**Site**	**x**	**y**	**z**	**U_{eq} (Å^2)**	**f_{occ}**
Rb	4*c*	0	0.6870(1)	0.250	0.062(1)	1
Cu	8*e*	0.8337(1)	0	0	0.061(1)	1
Br1	4*c*	0	0.1171(1)	0.25	0.0370(9)	1
Br2	8*g*	0.70912(8)	0.87708(8)	0.25	0.0574(8)	1
Atomic displacement parameters (Å^2)						
Atom	**U^{11}**	**U^{22}**	**U^{33}**	**U^{12}**	**U^{13}**	**U^{23}**
Rb	0.065(1)	0.082(1)	0.039(1)	0.00000	0.00000	0.00000
Cu	0.066(1)	0.060(1)	0.0578(9)	0.00000	0.00000	0.0146(8)
Br1	0.0355(8)	0.0367(1)	0.039(1)	0.00000	0.00000	0.00000
Br2	0.0577(8)	0.0788(9)	0.0355(7)	−0.0362(7)	0.00000	0.00000
R_p = 2.8%, R_{wp} = 4.8%, χ^2 = 11.4, R_{Bragg} = 3.6%						

Table S2: Crystallographic data for $RbCu_2Br_3$ phase in the orthorhombic $Cmcm$ space-group from SXRD at 200 K. Unit-cell parameters: a = 9.82574(6) Å, b = 12.36441(9) Å, c = 5.52373(3) Å, and V = 671.075(7) Å^3.

Atom	**Site**	***x***	***y***	***z***	**U_{eq} (Å^2)**	**f_{occ}**
Rb	4*c*	0	0.6884(1)	0.250	0.046(1)	1
Cu	8*e*	0.8343(1)	0	0	0.0485(9)	1
Br1	4*c*	0	0.1159(1)	0.25	0.0264(9)	1
Br2	8*g*	0.70862(8)	0.87560(8)	0.25	0.0453(8)	1
Atomic displacement parameters (Å^2)						
Atom	**U^{11}**	**U^{22}**	**U^{33}**	**U^{12}**	**U^{13}**	**U^{23}**
Rb	0.046(1)	0.052(1)	0.042(1)	0.00000	0.00000	0.00000
Cu	0.0500(9)	0.051(1)	0.0446(8)	0.00000	0.00000	0.0104(8)
Br1	0.0281(9)	0.0184(9)	0.033(1)	0.00000	0.00000	0.00000
Br2	0.0422(8)	0.0569(8)	0.0370(8)	−0.0287(6)	0.00000	0.00000
R_p = 6.5%, R_{wp} = 8.6%, χ^2 = 13.3, R_{Bragg} = 3.73%						

III. Prediction of acoustic and optical modes using group-theory

Table S3: Factor-group analysis for the $Cmcm$ crystal structure ($^{D_{2h}}$) of $RbCu_2Br_3$ halide.

Atom	Site	Symmetry	Irreducible representation
Rb	4*c*	$m2m$ (C_{2v}^{y})	$A_g \oplus B_{1g} \oplus B_{1u} \oplus B_{2u} \oplus B_{3g} \oplus B_{3u}$
Cu	8*e*	2.. (C_2^x)	$A_g \oplus A_u \oplus 2B_{1g} \oplus 2B_{1u} \oplus 2B_{2g} \oplus 2B_{2u} \oplus B_{3g} \oplus B_{3u}$
Br1	4*c*	$m2m$ (C_{2v}^{y})	$A_g \oplus B_{1g} \oplus B_{1u} \oplus B_{2u} \oplus B_{3g} \oplus B_{3u}$
Br2	8*g*	..m (C_s^{xy})	$2A_g \oplus A_u \oplus 2B_{1g} \oplus B_{1u} \oplus B_{2g} \oplus 2B_{2u} \oplus B_{3g} \oplus 2B_{3u}$
		Total	$5A_g \oplus 2A_u \oplus 6B_{1g} \oplus 5B_{1u} \oplus 3B_{2g} \oplus 6B_{2u} \oplus 4B_{3g} \oplus 5B_{3u}$
		Infrared	$4B_{1u} \oplus 5B_{2u} \oplus 4B_{3u}$
		Raman	$5A_g \oplus 6B_{1g} \oplus 3B_{2g} \oplus 4B_{3g}$
		Acoustic	$B_{1u} \oplus B_{2u} \oplus B_{3u}$
		Silent	$2A_u$

Table S4: Factor-group analysis for the $Pnma$ crystal structure ($^{D_{2h}}$) of $RbCu_2Br_3$ halide.

Atom	Site	Symmetry	Irreducible representation
Rb	4*c*	.m. (C_s^{xz})	$2A_g \oplus A_u \oplus B_{1g} \oplus 2B_{1u} \oplus 2B_{2g} \oplus B_{2u} \oplus B_{3g} \oplus 2B_{3u}$
Cu	8*d*	1 (C_1)	$3A_g \oplus 3A_u \oplus 3B_{1g} \oplus 3B_{1u} \oplus 3B_{2g} \oplus 3B_{2u} \oplus 3B_{3g} \oplus 3B_{3u}$
Br1	4*c*	.m. (C_s^{xz})	$2A_g \oplus A_u \oplus B_{1g} \oplus 2B_{1u} \oplus 2B_{2g} \oplus B_{2u} \oplus B_{3g} \oplus 2B_{3u}$
Br2	4*c*	.m. (C_s^{xz})	$2A_g \oplus A_u \oplus B_{1g} \oplus 2B_{1u} \oplus 2B_{2g} \oplus B_{2u} \oplus B_{3g} \oplus 2B_{3u}$
Br3	4*c*	.m. (C_s^{xz})	$2A_g \oplus A_u \oplus B_{1g} \oplus 2B_{1u} \oplus 2B_{2g} \oplus B_{2u} \oplus B_{3g} \oplus 2B_{3u}$
		Total	$11A_g \oplus 7A_u \oplus 7B_{1g} \oplus 12B_{1u} \oplus 11B_{2g} \oplus 7B_{2u} \oplus 7B_{3g} \oplus 11B_{3u}$
		Infrared	$10B_{1u} \oplus 6B_{2u} \oplus 10B_{3u}$
		Raman	$11A_g \oplus 7B_{1g} \oplus 11B_{2g} \oplus 7B_{3g}$
		Acoustic	$B_{1u} \oplus B_{2u} \oplus B_{3u}$
		Silent	$7A_u$

IV. Distortion-mode analysis

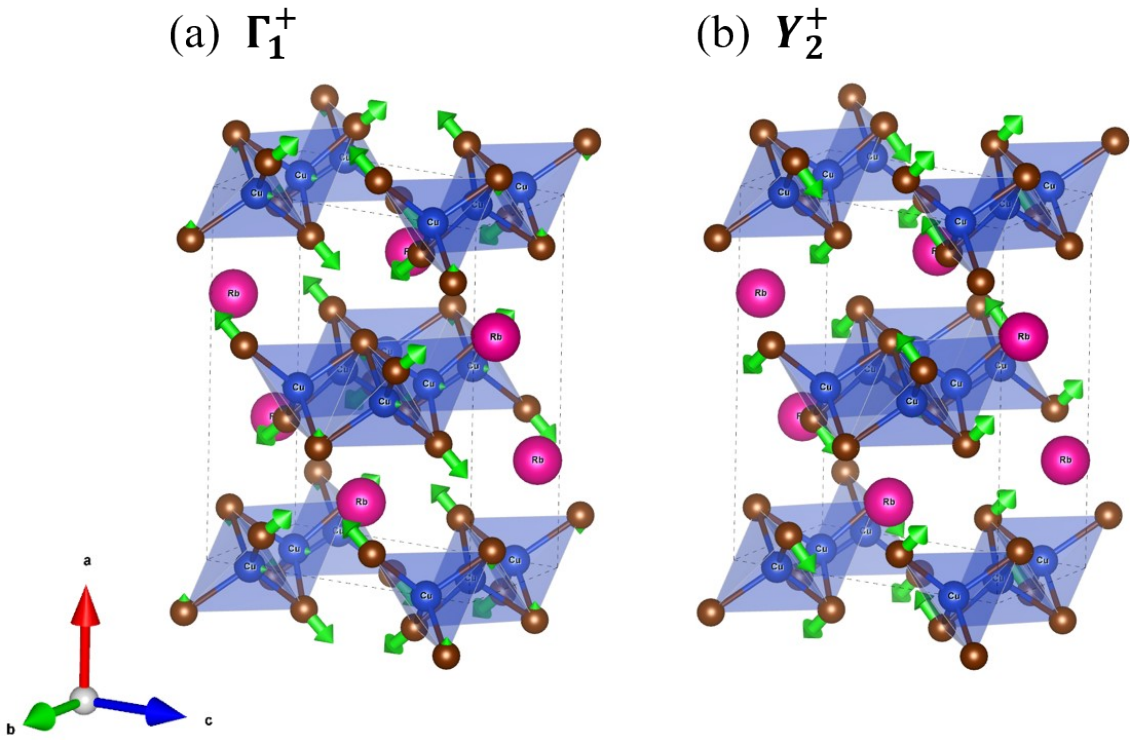

Fig. S7: Alternative view of the atomic displacement patterns for the symmetry-adapted modes involved in the $Cmcm \rightarrow Pnma$ transition of $RbCu_2Br_3$. Green arrows denote the direction and relative magnitude of the distortions. Bromide atoms are shown as brown spheres.

Table S5. Crystallographic data for $RbCu_2Br_3$ halide at 300 K defined in the orthorhombic $Cmcm$ (no. 63) space-group. Lattice parameters: a = 9.86677 Å, b = 12.44338 Å, and c = 5.5799 Å.

Atom	**Site**	***x***	***y***	***z***
Rb	4*c*	0	0.68874	0.25
Cu	8*e*	0.83606	0	0
Br1	4*c*	0	0.11628	0.25
Br2	8*g*	0.71052	0.87756	0.25

Table S6. Crystallographic data for $RbCu_2Br_3$ halide at 100 K defined in the orthorhombic $Pnma$ (no. 62) space-group. Lattice parameters: a = 12.3535 Å, b = 5.50066 Å, and c = 9.83121 Å.

Atom	**Site**	***x***	***y***	***z***
Rb	4*c*	0.68942	0.75	-0.0129
Cu	8*d*	0.4958	0.4982	0.33437
Br1	4*c*	0.38504	0.25	0.5075
Br2	4*c*	0.6103	0.25	0.191
Br3	4*c*	0.36135	0.75	0.2242

Using the low- and high-symmetry crystal structures as input, together with the transformation matrix reported below, one can reproduce the distortion-mode analysis carried out for $RbCu_2Br_3$ halide, as well as the detailed description of its structural phase transition.

Transformation matrix (P,p)**:** $\left(b,c,a;0,0,\frac{1}{2}\right)$

$$(P,p) = \begin{pmatrix} 0 & 0 & 1 & 0 \\ 1 & 0 & 0 & 0 \\ 0 & 1 & 0 & \frac{1}{2} \end{pmatrix}$$